Climate Migration Amplifies Demographic Change and Population Aging

Mathew E. Hauer *
Department of Sociology, Florida State University
and
Sunshine Jacobs
Department of Sociology, Florida State University
and
Scott Kulp
Climate Central

March 7, 2022

Abstract

The warnings of potential climate migration first appeared in the scientific literature in the late 1970s when increased recognition that disintegrating ice sheets could drive people to migrate from coastal cities. Since that time, scientists have modelled potential climate migration without integrating other population processes, potentially obscuring the demographic amplification of this migration. Climate migration could amplify demographic change – enhancing migration to destinations and suppressing migration to origins. Additionally, older populations are the least likely to migrate and climate migration could accelerate population aging in origin areas. Here, we investigate climate migration under sea-level rise (SLR), a single climatic hazard, and examine both the potential demographic amplification effect and population aging by combining matrix population models, flood hazard models, and a migration model built on 40 years of environmental migration in the US to project the US population distribution of US counties. We find that the demographic amplification of SLR for all feasible RCP-SSP scenarios in 2100 ranges between 8.6M - 28M [5.7M - 53M] – 5.3 to 18 times the number of migrants (0.4M - 10M). We also project a significant aging of coastal areas as youthful populations migrate but older populations remain, accelerating population aging in origin areas. Furthermore, our population projection approach can be easily adapted to investigate additional or multiple climate hazards.

Keywords: Climate Change, Human Migration, Demography, Multiregional population projections, Sea-level rise

*Thanks y'all!

1 Introduction

Thirty years ago, the IPCC raised concerns that climate change could "initiate large migrations of people'' (IPCC & WMO 1992). Projections suggest these large migrations could be more than 140 million people by 2050 (Rigaud et al. 2018) and up to 3 billion people could be left outside the human climate niche (Xu et al. 2020). The potential for widespread human migration in the face of climate change continues to be an adaptation policy priority (US White House 2021).

Despite the importance of climate migration as an adaptation strategy (Black et al. 2011), relatively few studies have attempted to model the demographic impact of climate migration. Previous attempts eschew two key considerations in modelling climate migration.

First, scientists have chosen to model migrants as age-less and sex-less individuals (Hauer 2017, Davis et al. 2018, De Lellis et al. 2021, Rigaud et al. 2018), ignoring the well-established relationship between migration propensity and demographic characteristics (Black et al. 2011, Clark & Maas 2015, Rogers 1988). In particular, the near universal age schedule of migration, with older populations the least likely age groups to migrate and young adults the most likely, suggests climate migration is most likely to occur among working-age adults. Significant climate migration literature focuses on migration among young, working-age adults (Seto 2011, Lilleør & Van den Broeck 2011, Shen & Gemenne 2011, Donner & Webber 2014). Origin areas could experience accelerated population aging as younger populations migrate in response to climate change and older populations remain (Matos-Moreno et al. 2021). By ignoring these well-established demographic relationships, the extent to which highly vulnerable communities could experience accelerated population aging from climate migration as more youthful populations migrate away remains under-explored.

Second, climate migration models lack the crucial feedback loop whereby climate migrants alter the demographic trajectory in both their origin and destination. If climate change forces people to migrate, a potential domino effect could result, enhancing population growth in destination areas and suppressing population growth in hazardous origin areas (Curtis & Schneider 2011, Hauer et al. 2020, Marandi & Main 2021). Scientists rarely

model this population compounding (see Rigaud et al. (2018) for a notable exception) and the extent to which climate migration will alter demographic futures remains unknown.

Sea-level rise (SLR) emerged as a potential driver of climate migration more than forty years ago (Mercer 1978) due to the potential disintegration of antarctic ice sheets. Since those early warnings, SLR has remained one of the most costly and visible impacts of global climate change (McGranahan et al. 2007, Nicholls 2011, Strauss et al. 2015). With the global coastal population projected to eclipse one billion people this century (Neumann et al. 2015), SLR is expected to affect and, in many cases, displace hundreds of millions of people (Hauer 2017, Nicholls 2011) making it one of the largest potential sources of climate migration.

In this paper, we combine matrix population models, flood hazard models, and a migration model built on 40 years of environmental migration to project the United States' population distribution, accounting for anticipated demographic change, migration probabilities, and SLR. This approach allows us to investigate the potential compounding or amplification of demographic change in both origin and destination communities and accelerated aging in coastal communities due to SLR.

To investigate climate migration, we produce three population populations using multiregional Leslie matrices that take the following general forms:

$$\begin{aligned} \text{Base} : \mathbf{P}_{t+1}^{Base} &= \mathbf{S}_t \mathbf{P}_t^{Base} \\ \text{Displacement} : \mathbf{P}_{t+1}^{Disp} &= \mathbf{M}_{ty} \mathbf{S}_t \mathbf{P}_t^{Base} \\ \text{Amplification} : \mathbf{P}_{t+1}^{Amp} &= \mathbf{M}_{ty} \mathbf{S}_t \mathbf{P}_t^{Amp} \end{aligned}$$

Where $\mathbf{P}_{t+1}$ is the population at time $t+1$, $\mathbf{S}_t$ is a Leslie matrix containing the age-sex specific probabilities of fertility and survival, $\mathbf{M}_{ty}$ is a matrix containing the proportion migrating from county to county under y amount of SLR. See **Methods** and **Supplementary Information** for details.

Our 'Base' population projection represents a projection agnostic to climate change. 'Displacement' represents a similar projection to those undertaken in the broader literature (e.g. Hauer (2017),Davis et al. (2018),Robinson et al. (2020)). This projection renders the displaced migrants demographically inert, preventing climate migrants from demographically interacting in their destinations but allowing migrants, and only migrants, to move

across space. Finally, our 'Amplification' population projection accounts for integrated population dynamics in origins and destinations.

We populate our matrices from multiple data sources. $\mathbf{P}_t$ comes from the National Vital Statistics System (NVSS) U.S. Census Populations with Bridged Race Categories Data set (`https://seer.cancer.gov/popdata/download.html`). $\mathbf{S}_t$ is populated with cohort-change ratios (CCRs) from the NVSS population data. Finally, $\mathbf{M}_{ty}$ contains the proportion migrating from each county to each county based on the IRS county-to-county migration data (Molloy et al. 2011) and adjusted to account for the h proportion of each county inundated by SLR.

$\mathbf{M}_{ty}$ reflects the percentage of population we anticipate will be displaced by SLR from a parsimonious displacement model. We arrive at this reduction with a simple, parsimonious model fit with US counties between 1980 and 2019 with SHELDUS verified large ($>4\sigma$) population declines (n=48 such county-years). We estimate exposure to SLR as a percentage of the population in each county using a bathtub model of inundation based on the population-weighted area under RCPs 2.6, 4.5, and 8.5 (for 2100 SLR amounts of 0.5 meters [0.29-0.82], 0.59 [0.36-0.93], and 0.79 [0.52-1.2] 90th percentile prediction intervals). For simplicity and clarity, we report most results using RCP4.5.

Finally, $\mathbf{M}_{ty}$ and $\mathbf{S}_t$ are projected using ARIMA(0,1,1) ($\mathbf{S}_t$) and ETS models ($\mathbf{M}_{ty}$) to capture potential changes in demographic rates.

2 Results

We find that RCP4.5 compromises the land area home to 8.6M - 28M [5.7M - 53M] [1] people between 2020 and 2100 (**Figure 1a** and **Figure 2**). In this simple model, the demographic impact of SLR manifests as 0.4M - 10M people migrating to other places for a net demographic change of 0.4M - 10M people ('Displacement' model). However, when one accounts for population dynamics ('Amplification' model), the actual *demographic* impact of 0.4M - 10M migrants is 8.6M - 28M. This is due to two interacting effects: a compounding or 'domino effect' where destination counties attract more people over time and origin

[1] Unless otherwise stated, uncertainty intervals in parentheses relate to SSP3-RCP4.5 5th percentile and SSP5-RCP4.5 95th percentile.

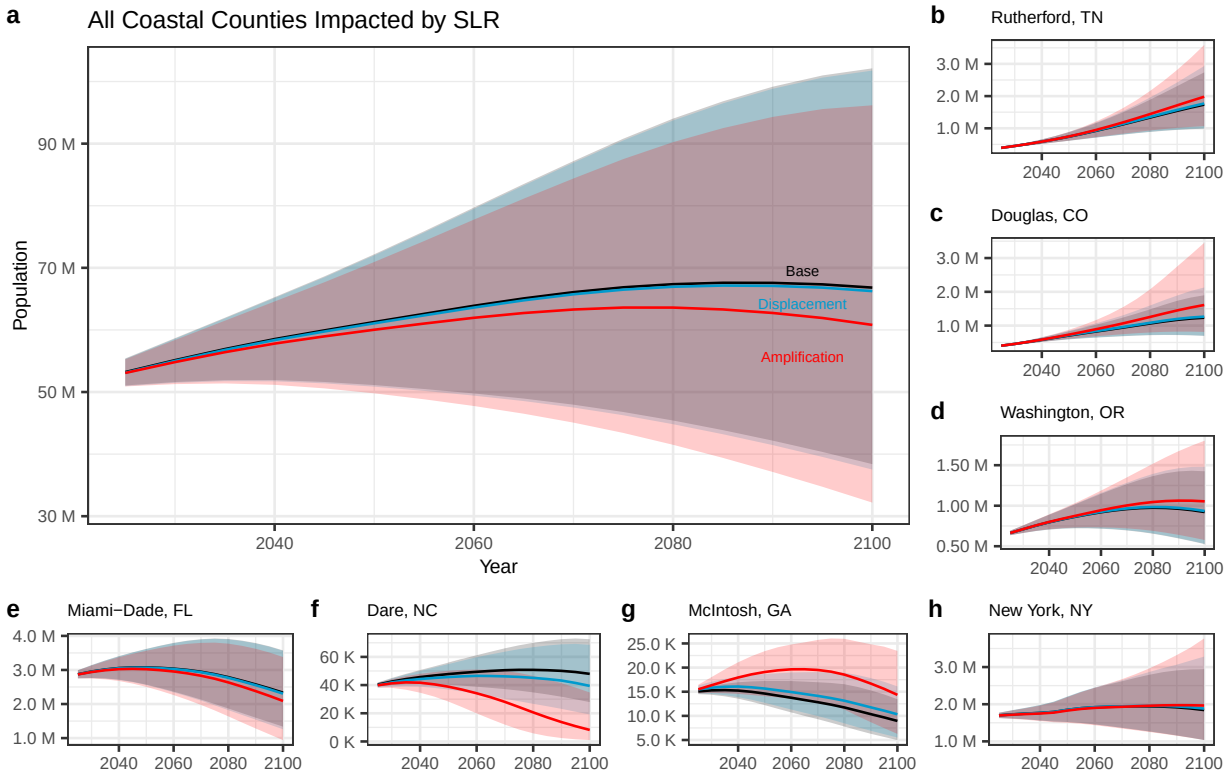

Figure 1: **A comparison of base, inundation, and migration projections for all US coastal counties impacted by sea-level rise and other example counties over the next century.** These projections use RCP4.5. Uncertainty reflects the 95th percentile prediction interval and the minimum/maximum SSP. We adopt the general climate migration typology as proposed by (Marandi & Main 2021) for the seven example counties. (a) compares the population trajectories for all US coastal counties impacted by SLR. Here we can see the amplification effect of population processes and migration, driving population much lower than a simple displacement model suggests. (b-d) are example 'Destination' counties using (Marandi & Main 2021)'s framework. (e-f) are example 'Vulnerable' counties, showing significant declines earlier in the century. (g-h) are example 'Recipient' counties. The integrated demographic model (Amplification) exhibits significant amplification of the demographic trajectories, depending on the timing and extent of inundation.

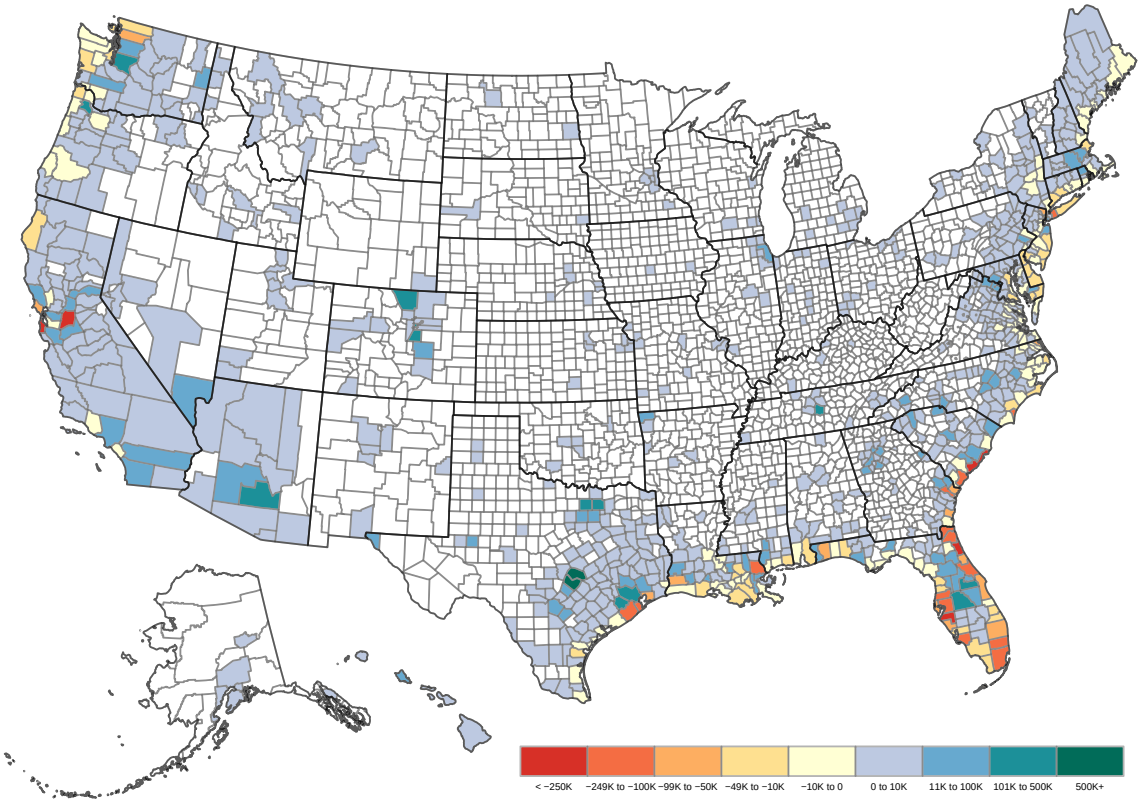

Figure 2: **Projected numeric change in population due to amplified population processes under SSP2-RCP4.5 50th percentile in 2100.** This map highlights the 'domino effect' where climate migration further enhances migration to destinations and suppressing migration to origins.

counties attract less and the interaction of migrants with the other demographic component processes of fertility and mortality. This total demographic effect is considerably more pronounced than the simple displacement effect – 5.3 to 18 times larger. Under all plausible RCP-SSP scenarios except RCP4.5-SSP3, SLR leads to a demographic amplification of at least 10 million persons (**Table 1**.

Furthermore, **Figure 1** shows this population compounding effect for seven example counties following the general typology of climate migration put forth by (Marandi & Main 2021). Here, **Figure 1e-f** are counties experiencing significant population declines over the

Table 1: **RCP-SSP matrix for 2100 showing all feasible RCP-SSP combinations** (O'Neill et al. 2016). Here we compare the expected number of migrants with the demographic amplification for all reasonable RCP-SSP combinations. All numbers in parentheses are the 90th percentile prediction interval. Regardless of the RCP-SSP combination, matrix population models suggest millions of people will shift in the United States due to sea-level rise.

RCP		SSP1	SSP2	SSP3	SSP4	SSP5
	SLR Amount (meters)			0.79 [0.52 - 1.2]		
8.5	Migrants (millions)					3.4 [1.3 - 10]
	Demographic Amplification (millions)					28 [17 - 53]
	SLR Amount (meters)			0.59 [0.36 - 0.93]		
4.5	Migrants (millions)	1.5 [0.65 - 4.2]	1.5 [0.63 - 4.1]	0.84 [0.36 - 2.3]	1.2 [0.51 - 3.3]	2.2 [0.96 - 6.2]
	Demographic Amplification (millions)	15 [10 - 27]	15 [10 - 26]	8.6 [5.7 - 15]	12 [8 - 21]	23 [15 - 41]
	SLR Amount (meters)			0.5 [0.29 - 0.82]		
2.6	Migrants (millions)	1.2 [0.55 - 3.5]	1.2 [0.54 - 3.4]		0.96 [0.44 - 2.8]	1.8 [0.82 - 5.1]
	Demographic Amplification (millions)	14 [9.7 - 24]	14 [9.5 - 24]		11 [7.6 - 19]	21 [15 - 37]

entire time horizon. Our results for Miami-Dade FL under RCP4.5 suggests 28.3K [4.4K - 204.2K] migrants by 2100 but a total demographic impact of 243.9K [72.9K - 1.1M] fewer people. We see similar results for Dare NC as well (8.5K [1.5K - 22.9K] migrants and a 39.8K [14.6K - 70.0K] total demographic impact).

Figure 1g-h are counties close to heavily threatened areas. We see two separate population trajectories and demonstrate the amplification of population change. McIntosh GA is initially a 'climate destination', as people from nearby heavily effected areas migrate into nearby counties. But as the century wears on, this 'climate destination' turn into a vulnerable county and migration begins to turn into negative population growth. The difference between the simple, 'Displacement' model and the demographically integrated 'Amplification' model suggests population growth trajectories in opposing directions, where the 'Displacement' model has McIntosh growing into the end of the century whereas the 'Amplification' model has it declining. These results suggest that many people and their descendants could find themselves exposed and displaced by SLR as presently safe areas become increasingly vulnerable over time. In the case of New York NY, SLR initially takes people away from the county before population growth turns positive in the tail end of the century, transitioning from a 'Vulnerable County' to a potential 'Climate Destination'.

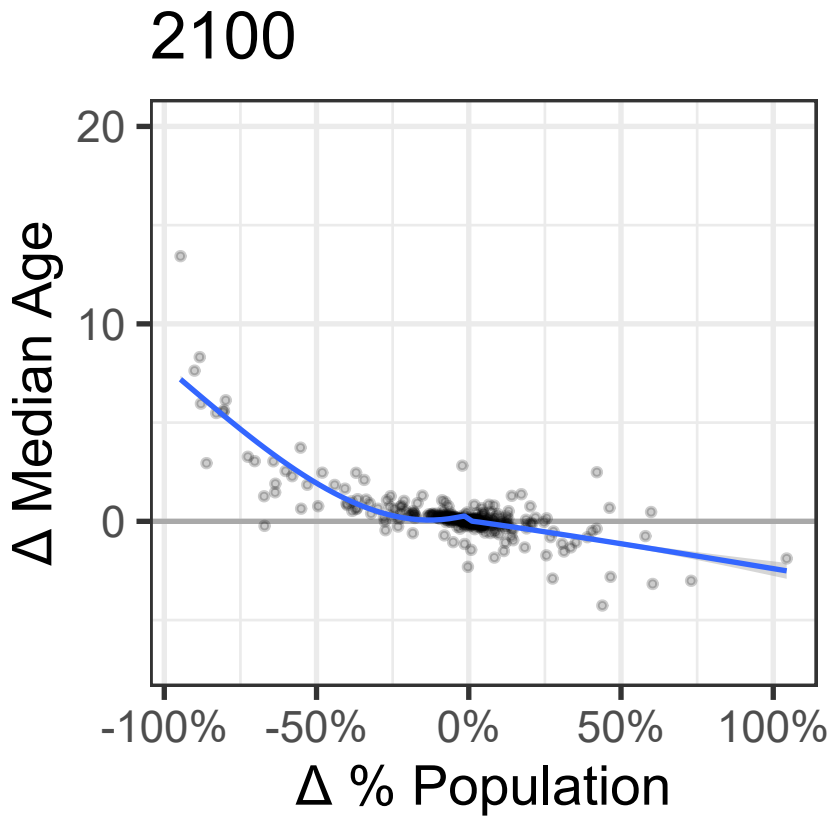

Figure 3: **Population Aging and climate migration**. Here we show he relationship between population decline due to SLR and aging by 2100. The more an area experiences climate out-migration, the greater the population aging. Conversely, the more an area experiences climate in-migration, the younger the area becomes. Results shown are under SSP2-RCP4.5 50th percentile.

Finally, **Figure 1b-d** are examples of 'Climate Destinations' (counties considered 'climate havens'). We see a similar, though reversed, pattern of population trajectories to 'Vulnerable Counties.' Here, Rutherford TN (245.1K [78.5K - 852.3K] amplified demographic change versus 34.9K [8.2K - 197.5K] displaced migrants), Douglas CO (377.7K [117.8K - 1.6M] vs. 32.3K [5.2K - 230.3K]), and Washington OR (131.9K [50.9K - 377.8K] vs. 12.9K [3.8K - 55.1K]) exhibit considerably larger demographic impacts when accounting for population dynamics compared to just the displacement model. These results echo suggestions of emerging climate havens in 'safer' areas (Marandi & Main 2021).

Figure 3 shows the impact of population processes on aging related to climate migra-

tion. We find that as the percentage of the population lost due to climate migration-related population processes increases, the median age in the population also increases (**Figure 3**). Conversely, counties receiving the greatest increase actually exhibit more *youthful* populations. This effect is particularly pronounced in some counties where the increase in median age can approach 10+ years in some highly impacted coastal counties due to climate migration.

3 Discussion

Climate migration continues to receive both policy and scientific focus. But projections of climate migration that do not account for other population processes fail to describe compounding population effects or accelerated population aging in origins. When population processes are fully integrated within a climate migration model, we see dramatic impacts on both origin and destination communities, particularly in their changing age structures.

Given our results, vulnerable areas experiencing climate out-migration could face a future where more youthful age groups exercise 'migration as adaptation' but the oldest populations remain in vulnerable areas. Climate migration could place an enormous burden on those communities' that might face the triple challenges of climate change, dwindling populations, and rapid population aging. Adaptation costs continue to rise (Buchner et al. 2014) but communities could struggle to afford the necessary adaptation strategies to protect their remaining residents as prime-age income earners migrate away, potentially eroding local tax bases.

Furthermore, given the accelerated population aging in origin communities, maladaptation could easily result if adaptation strategies are aimed at more youthful populations who are less likely to remain in these areas. Some adaptation strategies to build resiliency to SLR call for raising first floor elevations (Dedekorkut-Howes et al. 2020) yet elevating homes and adding steps might result in maladaptation in communities facing accelerated aging due to climate migration.

Destination communities also face challenges due to climate migration. Destination communities that only consider climate migrants underestimate the population change likely to occur due to demographic compounding effects. Climate destinations are likely to

become even more attractive as additional gravity driven migration effects play a crucial factor for additional migration streams, beyond just climate migrants. For some climate destinations already struggling with growth management and sustainability goals, climate migration poses significant challenges. The total demographic impact of climate migration could further burden these communities if growth is managed haphazardly. Destination communities for climate migrants should consider these other demographic forces in their sustainability plans and address challenges sooner rather than later.

Climate migration has been broadly conceptualized as simply a rearrangement of people across space. Our results show that this conceptualization underestimates the total demographic impact in two main ways: climate migration is likely to accelerate population aging in origins and accelerate population growth in destinations. We also demonstrate that climate migration in isolation is unlikely to significantly alter population distributions but climate migration in combination with other population processes *will* produce significant demographic shifts in the future. This work offers the first glimpse of these demographic shifts.

We model RCPs 2.6, 4.5, and 8.5 which imply a maximum 2100 SLR amount at 1.2m under RCP8.5 (Kopp et al. n.d.). While these SLR amounts are in line with recent IPCC projections, other SLR projections suggest 2100 SLR could greatly exceed 1.2m (Rahmstorf 2007, Bamber et al. (2019),Sweet et al. (2017)). It is possible that the demographic amplification we find is likely conservative. We also choose to model migration resulting from complete inundation yet it is possible migration begins sooner than complete inundation (Hauer et al. 2020). Thus, the direct migration we model could also be considered conservative. If people migrate sooner, in a more anticipatory manner, the demographic amplification we find would be understated. –>

Additionally, the approach for modeling the demographic implications of climate migration shown here allows for modelling demographic change in concert with other climate stressors – not just SLR. Our parsimonious, one-dimensional displacement model requires minimal translation of climate hazards into age-specific displacement. Future scientists could implement extreme heat/humidity combinations, tropical cyclones, or water availability as either singular climate hazards or in a multi-hazard model. To our knowledge,

few, if any, demographic projection models account for climate change impacts. This type of modelling approach has great potential to better understand the integration of population processes and climate change.

4 Acknowledgements

This work was supported by the State of Louisiana, the American Society of Adaptation Professionals, the New York State Energy Research & Development Authority, and the Great Lakes Integrated Sciences & Assessment. We would like to thank T. Gill, N. Nagle, A. Moulton, S. Bohon, C. Schmertmann, and E. Fenimore, for their early feedback and assistance. Thank you!

5 Methods and Materials

We employ the use of multiregional Leslie matrices (Rogers 1966) to project climate migration in the United States. **Equation 1** is the general form for our projections.

To answer our research questions, we employ three main modules. The first is the development of a parsimonious, one-dimensional, age-specific displacement model. The second is a sea-level rise exposure model. The third is a multiregional Leslie matrix specification.

5.1 Parimonious, one-dimensional, age-specific displacement model

Our displacement model makes use of a statistical time series outlier detection technique to first identify anomalous demographic behavior in a time series and then verify that this anomalous behavior is associated with an environmental event.

We use a statistical time series outlier detection algorithm (Chen & Liu 1993), implemented in the R programming language (R Core Team 2019) via the tsoutliers package (López-de-Lacalle 2019).

This algorithm iteratively uses ARIMA models to 1) identify potential outliers and 2) refit the ARIMA with the outliers removed to produce a counter-factual time series. First, an ARIMA model is fit to the time series using the `forecast` package in R (Hyndman et al.

2019, Hyndman & Khandakar (2008)) where the best performing ARIMA model is selected based on the Bayesian information criterion (BIC). Finally, the residuals from the forecast are checked for their significance where only outliers above a critical t-static are considered "true'' outliers ($|\tau| \geq 4$; p-value < 0.000063). We chose this threshold to minimize the probability of committing a Type I error (or claiming an outlier is true when it is, in fact, not).

We use this outlier detection algorithm to search over county population totals for the time period 1980-2019. We use the National Vital Statistics System (NVSS) U.S. Census Populations with Bridged Race Categories data set. The NVSS Bridged Race Categories data set harmonizes racial classifications across disparate time periods to allow population estimates to be sufficiently comparable across space and time. Importantly, all county boundaries are rectified to be geographically consistent across all time periods. We use the the 1969-2019 data set, but the historical population estimates prior to 1980 display unusual volatility, so we consider only the time periods 1980-2019. We also only consider counties created prior to year 2000 and contained in the NVSS data.

We search all US counties for negative statistical outliers (indicating population losses) between 1980 and 2019. We detect 52 county-years with population losses of magnitude 4σ or greater. We then use the Spatial Hazard Events and Losses Database for the United States (SHELDUS) (for Emergency Management and Homeland Security 2018), a county-level hazard data set for the US which contains information about the direct losses (property and crop losses, injuries, and fatalities) caused by a hazard event (thunderstorms, hurricanes, floods, wildfires, tornadoes, flash floods, earthquakes, etc.) for the period 1960 to the present. We use SHELDUS to ensure the county time periods we identify as statistical outliers with population losses experienced an environmental hazard in that county-year with per capita hazardous losses in excess of the 50th percentile. This is to ensure the outlier population losses that we detect are associated with a hazard rather than other forces, such as economic forces.

Four county-periods either were not in the SHELDUS database or experienced per capita hazard losses below the 50th percentile. Additionally, one county-period contained age-sex groups with 0 people, necessitating exclusion. The remaining 48 environmental

events include tornadoes, wind damage, winter weather, earthquakes, flooding, tropical cyclones, hail, and other environmental hazards. Using this universe of 48 county-periods exhibiting large population declines after verified hazard losses, across over 40 years and across a wide variety of environmental hazards, we then build a flexible, one-dimensional, age-specific displacement model.

To link population displacement with age-specific population changes, we calculate cohort-change ratios (CCRs) in each county using the NVSS population data for the period 1969-2019. Cohort-change ratios take the following general form (see (Hauer 2019, Swanson et al. (2010)) for a more detailed description):

$$CCR_{x,t} = \frac{{}_nP_{x,t}}{{}_nP_{x-k,t-k}} \tag{2}$$

Where ${}_nP_{x,t}$ is the population aged x to $x+n$ in time t and ${}_nP_{x-k,t}$ is the population aged $x-k$ to $x+n-k$ in time t where k refers to the time difference between time periods. Since mortality must decrement a population, any CCR above 1.0 implies a net-migration rate in excess of the mortality rate, and a growing population. There is special consideration for both the initial age group without a preceding age group and the final, open-ended age interval without a proceeding age group (see (Hauer 2019) for additional details).

We build the following model based on the relationship between the change in CCRs at age x, $\Delta CCR_x = CCR_{x,t}/CCR_{x,t-1}$, and the percentage decline in the total population compared to the counter-factual in the outlier detection method, $\Delta P_t = \hat{P}_t/P_t$:

$$log(\Delta CCR_x) = a_x + b_x h + c_x h^2 \tag{3}$$

Here, h is the $\log(\Delta P_t)$ and shows a quadratic relationship with the logarithm of the change in CCRs by age. x refers to five-year age groups: 0-4, 5-9,..., 85+. This is a similar model and approach to Wilmoth et al.'s (Wilmoth et al. 2012) flexible, one-dimensional mortality model based on the similarity between age-specific mortality rates and infant mortality. **Table S1** depicts the correlation coefficients between $\log(\Delta CCR_x)$ and $\log(\Delta P_t)$. The age groups with the lowest correlation coefficients are young adult males aged 20-39 and those in the open-ended age interval (80+), suggesting these age/sex groups react to environmental signals the least predictably.

Using $h_{ty} = log(\Delta P_{ty})$, we can estimate age-specific changes in CCRs after an environmental event by simply applying the following formula:

$$\hat{CCR}_{xy,t} = CCR_{x,t-1} \cdot e^{\hat{\beta}_x h_{ty} + \hat{c}_x h_{ty}^2} \quad (1)$$

Where $e^{\hat{\beta}_x h_{ty} + \hat{c}_x h_{ty}^2}$ provides the percentage change in CCR_{xt} based on the $\log(\Delta P_{ty})$ under SLR amount y. In this case, we drop the intercept (a_x) from the estimation procedure to ensure a 0% decline in population yields a corresponding 0% change in the CCR. Multiplying the result from the model with the CCR in the year prior yields the anticipated change in the CCR. These changes in CCRs can then be applied to any time series of population values to generate an anticipated population.

We estimate the predicted population using the equation outlined above and then compare it against the observed population. **Figures S1, S2**, and **Table S1** show the accuracy of our fitted, one-dimensional model. Regarding the total population in our 48 counties, our model performs well with an r^2 value of 0.996 and performs well regardless of population size. Regarding each individual P_x group, our model still performs quite well with an r^2 of 0.995. Just like with the total population, the accuracy of our model does not depend on population size.

5.2 Sea-level Rise Exposure

To estimate the populations at-risk to SLR and thus the value h in Equation 1, we employ inundation modeling (Hauer et al. 2020) which assumes that people who are underwater 100% of the time must migrate. We estimate these populations using airborne lidar-derived digital elevation models (DEMs) produced by NOAA and supplemented with both the USGS Northern Gulf of Mexico Topobathymetric DEM in Louisiana and the USGS National Elevation Dataset in the fraction of land not covered by other sources (see (Kulp & Strauss 2019) for details on the construction of the DEMs).

Using a bathtub model of inundation, we calculate the land area under a given water height to generate binary inundation surfaces. SLR exposure is hyperlocalized and we generate this inundation area in the Census Block Groups (CBG; n=81,815) located in coastal counties (n=406) expected to experience any probability of flooding. We use probabilistic

SLR projections (Sweet et al. 2017, Kopp et al. 2014) that are closely aligned with the IPCC for our water heights. To calculate the land area under a given water height, we simply threshold the DEM to find pixels below SLR_{yt} where y is the projected height of SLR in a given year t. For each CBG, we simply calculate the percentage of its pixels on dry land (defined in the National Wetland Inventory (U.S. Fish and Wildlife Service 2012)) covered by the inundation surface and multiply this percentage by the total population in the CBG in year t to produce the total number of people at-risk to a given amount of SLR in a given year. We then aggregate these CBGs to the county-level to calculate the percentage of people in a given county at-risk of inundation.

To account for potential sub-county shifts in population, we use the specification of sub-county demographic projections (Hauer et al. 2016). Specifically, we use a sub-county demographic projection to produce spatiotemporally consistent CBG boundaries for the period 1940-2010 and project these populations forward using a mixed, linear/exponential projection for the period 2010-2100. CBGs expected to increase use a linear projection and CBGs expected to decrease use an exponential projection. This creates a time-varying, population-weighted estimate of exposure to SLR.

The percentage of the population at-risk to SLR in each county, in essence, represents the ΔP_t from our Equation 1 above where $\Delta P_t = P_{t,y}/P_t$. In this case, $P_{t,y}/P_t$ is the percentage of the population in any county at-risk of inundation under a given water height y. Such a calculation allows us to seamlessly combine our parsimonious displacement model with our matrix population model.

5.3 matrix Population Models

We employ the use of multiregional Leslie matrices in our population projections (Rogers 1966).

Where $\mathbf{P}_t$ refers to the population matrix containing x age groups and $\mathbf{S}_t$ contains the age-specific fertility (F) and mortality rates (S), where S_x refers to the survival probabilities for age group x and F_x refers to the fertility rates.

We populate our Leslie matrices with the 3,143 US counties, 18 five-year age groups, and two sex groups, thus, $\mathbf{P}_t$ is a vector of length 113,148, and $\mathbf{S}_t$ and $\mathbf{M}_{ty}$ are 113,148

x 113,148 matrices. We use CCRs to populate our S_x values in each matrix and child-woman ratios to populate our F_x values. The values come from the NVSS Bridged Race Categories dataset. To project the CCRs, We employ an autoregressive integrated moving average (ARIMA) model for forecasting equally spaced univariate time series data. We use an `ARIMA(0,1,1)` model, which produces forecasts equivalent to simple exponential smoothing. All projections were undertaken in R (R Core Team 2019) using the `forecast` package (Hyndman et al. 2019).

We use the NVSS data for the period 1969-2019 for county c, age group x, sex s in an `ARIMA(0,1,1)` to create CCR_{cxst} for time periods $t+1$. The initial $\mathbf{P}_1$ and $\mathbf{S}_t$ matrices use the 2019 NVSS data.

We also calculate the probability of migrating from each county to each county and use this to populate the $\mathbf{M}_{ty}$ matrix. These data come from the IRS county-to-county migration files for 1990-2018 (see (Hauer & Byars 2019, DeWaard et al. 2021) for descriptions of this data). We populate $\mathbf{M}_{ty}$ as $M_t \cdot (1 - e^{\hat{\beta}_x h_{ty} + \hat{c}_x h_{ty}^2})$ and where $i = j$ as $e^{\hat{\beta}_x h_{ty} + \hat{c}_x h_{ty}^2}$. M_t is a vector containing the proportion migrating from county i to county j in the IRS migration data, thus ensuring the columns of $\mathbf{M}_{ty}$ sum to 1.0.

To capture changes in the migration system, we employ an ETS model (Error, Trend, Seasonal), a univariate time series forecasting model (Hyndman et al. 2008). We use an ETS model for migration instead of an ARIMA(0,1,1) as we do for the CCRs because the CCRs are subject to multiplication during a drift, whereas the migration system is not. A CCR that drifts from $1.1 \rightarrow 1.3$ represents more than a 10-fold increase in a projected population over our time horizons (1.1^{17} = 5x, 1.3^{17} = 86x). Projecting the migration system itself is not subject to such exponential drift.

We fit individual ETS models for each county's numeric migrants between each origin-destination dyadic pair using the `forecast` package in R (Hyndman et al. 2019). This approach allows the underlying migration system to evolve and change over the projection horizon, allowing dyadic pairs to wax or wane. We convert the numeric projections to fractions of the total projected migrants to populate the diagonal in the $\mathbf{M}$ matrix above where non-migrants (i.e. those migrating from $i \rightarrow i$) are included. The result is the fraction of individuals surviving from age group x who migrate from $i \rightarrow j$.

We control all population projections to the Shared Socioeconomic Pathways (Samir & Lutz 2017) and we use RCPs 2.6, 2.5, and 8.5 for our inundation scenarios (Kopp et al. 2014).

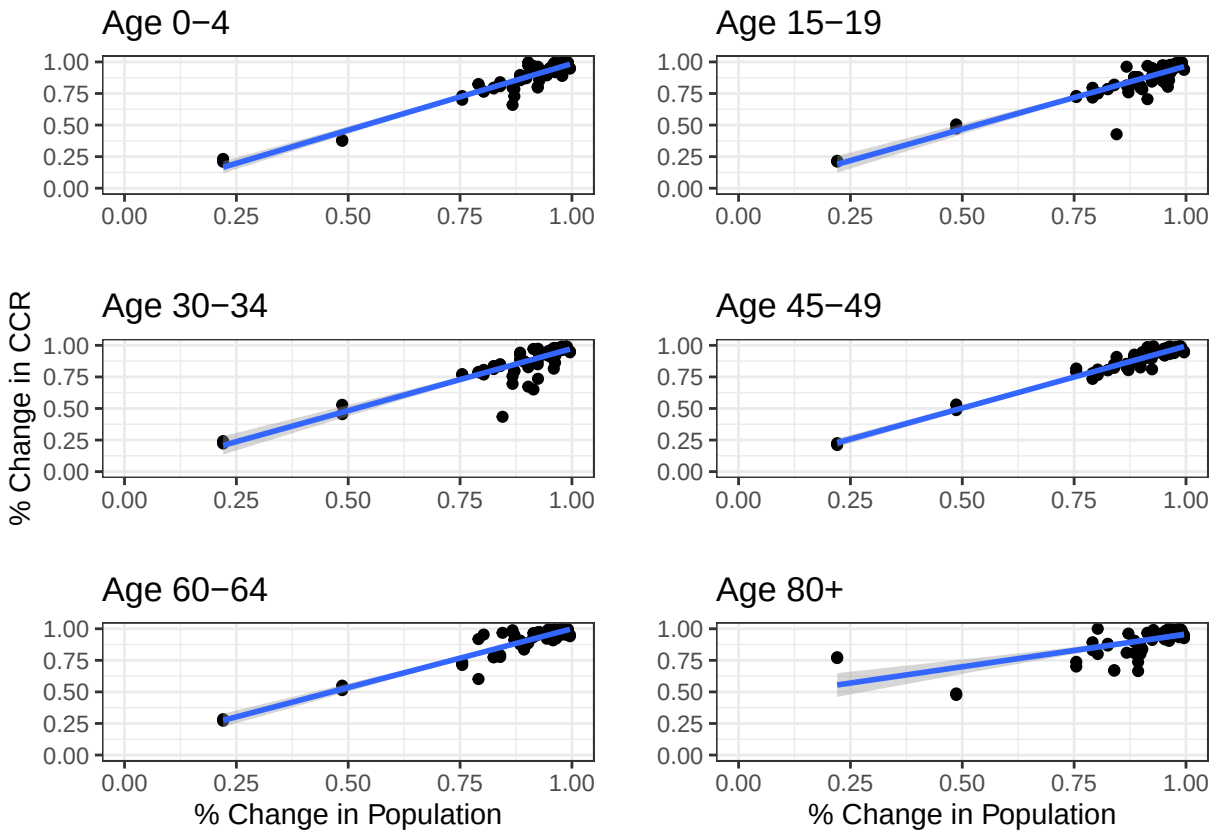

Figure 4: **Age-specific changes in cohort-change ratios vs. change in total population for selected age groups.**

6 Supplementary Information

6.1 Matrix Population Projections

To investigate SLR migration, we produce three separate population projections using a multi-regional Leslie matrix that takes the following general form

$$\begin{aligned} \text{Base} \quad &: \mathbf{P}_{t+1}^{Base} = \mathbf{S}_t \mathbf{P}_t^{Base} \\ \text{Displacement} \quad &: \mathbf{P}_{t+1}^{Disp} = \mathbf{M}_{ty} \mathbf{S}_t \mathbf{P}_t^{Base} \\ \text{Amplification} \quad &: \mathbf{P}_{t+1}^{Amp} = \mathbf{M}_{ty} \mathbf{S}_t \mathbf{P}_t^{Amp} \end{aligned} \tag{2}$$

In this section, we provide examples for all three projections. We will use a simplified example for a two-region population containing three age groups where each age group in

Table 2: **Correlation coefficients of changes in Cohort Change Ratios vs. Total Population Change (n=48).**

Age Group	Male	Female
0-4	0.932	0.944
5-9	0.959	0.934
10-14	0.963	0.962
15-19	0.805	0.925
20-24	0.656	0.919
25-29	0.710	0.932
30-34	0.754	0.957
35-39	0.870	0.974
40-44	0.927	0.960
45-49	0.966	0.958
50-54	0.963	0.972
55-59	0.962	0.956
60-64	0.894	0.890
65-69	0.813	0.916
70-74	0.934	0.824
75-79	0.840	0.802
80+	0.466	0.646

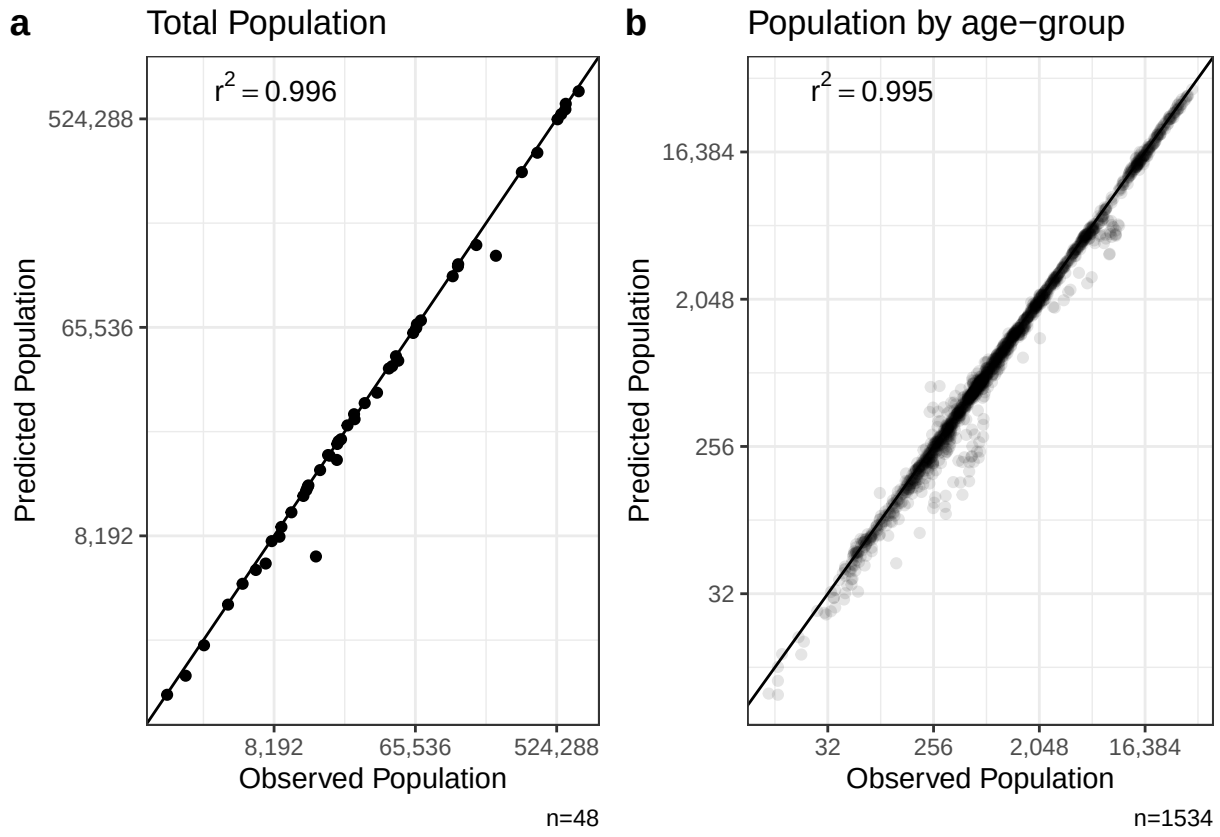

Figure 5: **Relationship between predicted populations using our model and observed populations in the 48 counties in our selection.** (a) shows the total population and (b) shows the populations for each age/sex group. The diagonal solid line is y=x. The model produces good fits for both the total population and by age/sex group.

region 1 contains 100 individuals and each age group in region 2 contains 200 individuals.

6.1.1 Base Projection

We employ the use of multiregional leslie matrices in our population projections.

In a typical Leslie matrix,

$$\mathbf{P}_{t+1} = \mathbf{S}_t \cdot \mathbf{P}_t \tag{5}$$

Where $\mathbf{P}_t$ refers to the population vector containing x age groups and $\mathbf{S}_t$ contains the age-specific fertility and mortality rates.

In a population with three age groups, production of a population projection looks akin to

$$\mathbf{P}_{t+1} = \begin{bmatrix} 0 & F_2 & F_3 \\ S_1 & 0 & 0 \\ 0 & S_2 & S_3 \end{bmatrix} \cdot \begin{bmatrix} P_1 \\ P_2 \\ P_3 \end{bmatrix}$$

where S_x refers to the survival probabilities for age group x and F_x refers to the fertility rates. In practice, we populate S_x using cohort-change ratios described in the Main Text.

These two matrices ($\mathbf{S}_t$ and $\mathbf{P}_t$) for our example populations take the following forms.

$$\mathbf{P}_t = \left[\begin{array}{c} 100 \\ 100 \\ 100 \\ \hline 200 \\ 200 \\ 200 \end{array}\right] \tag{3}$$

$$\mathbf{S}_t = \left[\begin{array}{ccc|ccc} 0 & 0.2 & 0.2 & 0 & 0 & 0 \\ 1.05 & 0 & 0 & 0 & 0 & 0 \\ 0 & 0.35 & 0.35 & 0 & 0 & 0 \\ \hline 0 & 0 & 0 & 0 & 0.2 & 0.2 \\ 0 & 0 & 0 & 0.98 & 0 & 0 \\ 0 & 0 & 0 & 0 & 0.33 & 0.33 \end{array}\right] \tag{4}$$

Thus, the 'Base' population projection produces

$$\mathbf{P}_{t+1} = \left[\begin{array}{ccc|ccc} 0 & 0.2 & 0.2 & 0 & 0 & 0 \\ 1.05 & 0 & 0 & 0 & 0 & 0 \\ 0 & 0.35 & 0.35 & 0 & 0 & 0 \\ \hline 0 & 0 & 0 & 0 & 0.2 & 0.2 \\ 0 & 0 & 0 & 0.67 & 0 & 0 \\ 0 & 0 & 0 & 0 & 0.33 & 0.33 \end{array}\right] \cdot \left[\begin{array}{c} 100 \\ 100 \\ 100 \\ \hline 200 \\ 200 \\ 200 \end{array}\right]$$

$$\mathbf{P}_{t+1} = \left[\begin{array}{c} 40 \\ 105 \\ 70 \\ \hline 80 \\ 196 \\ 132 \end{array}\right] \tag{5}$$

Here we would project region 1's population to go from 300 individuals in period 1 to 215 individuals in period 2 and region 2's population to go from 600 individuals to 408.

6.1.2 Displacement and Amplification Models

Our Displacement and Amplification models are similar but utilize multiregional Leslie matrices. In a multi-regional projection model, we can use a "super-matrix."

A 2-region model would take the following general form for the $\mathbf{S}_t$ matrix,

$$\mathbf{MS}_t = \left[\begin{array}{c|c} \mathbf{S}_i & \mathbf{M}_{j\to i} \\ \hline \mathbf{M}_{i\to j} & \mathbf{S}_j \end{array}\right]$$

Such that the diagonal $\mathbf{S}$ matrices contain combined survival, fertility, and migration probabilities while the off-diagonal $\mathbf{M}$ matrices contain the probabilities of each age-group moving from one region i to region j.

Here, we use the population vector resulting from the *Base* projection for our Displacement model and a new matrix, $\mathbf{M}_{ty}$, which contains the probability of migrating from one region to another. In a two region projection, 100% of migrants move from region 1 to region 2 and vice versa and 0% of migrants are non-movers (ie, region 1 $\rightarrow$ region 1). For

this example, Region 1 experiences 10% of its land area inundated by SLR ($h = 0.10$) and Region 2 experiences 0% of its land inundated by SLR. We populate the diagonal with the result of the parsimonious displacement model but for illustrative purposes, we assume that the result is equal to h. In practice, the value depends on both h and the specific age group x, ultimately resulting from $e^{\hat{\beta}_x h_{ty} + \hat{c}_x h_{ty}^2}$.

$$\mathbf{M}_{ty} = \left[\begin{array}{ccc|ccc} 0.9 & 0 & 0 & 0 & 0 & 0 \\ 0 & 0.9 & 0 & 0 & 0 & 0 \\ 0 & 0 & 0.9 & 0 & 0 & 0 \\ \hline 0.1 & 0 & 0 & 1 & 0 & 0 \\ 0 & 0.1 & 0 & 0 & 1 & 0 \\ 0 & 0 & 0.1 & 0 & 0 & 1 \end{array}\right] \tag{6}$$

Multiplying $\mathbf{M}_{ty}$ with $\mathbf{S}_t$ produces a combined migration/survival matrix that when multiplied by $\mathbf{P}_t$ yields the projected population.

$$\mathbf{M}_{ty}\mathbf{S}_t = \left[\begin{array}{ccc|ccc} 0 & 0.18 & 0.18 & 0 & 0 & 0 \\ 0.945 & 0 & 0 & 0 & 0 & 0 \\ 0 & 0.315 & 0.315 & 0 & 0 & 0 \\ \hline 0 & 0.02 & 0.02 & 0 & 0.2 & 0.2 \\ 0.105 & 0 & 0 & 0.98 & 0 & 0 \\ 0 & 0.035 & 0.035 & 0 & 0.33 & 0.33 \end{array}\right] \tag{7}$$

$$\mathbf{P}_{t+1} = \left[\begin{array}{ccc|ccc} 0 & 0.18 & 0.18 & 0 & 0 & 0 \\ 0.945 & 0 & 0 & 0 & 0 & 0 \\ 0 & 0.315 & 0.315 & 0 & 0 & 0 \\ \hline 0 & 0.02 & 0.02 & 0 & 0.2 & 0.2 \\ 0.105 & 0 & 0 & 0.98 & 0 & 0 \\ 0 & 0.035 & 0.035 & 0 & 0.33 & 0.33 \end{array}\right] \cdot \left[\begin{array}{c} 100 \\ 100 \\ 100 \\ \hline 200 \\ 200 \\ 200 \end{array}\right] = \left[\begin{array}{c} 36 \\ 94.5 \\ 63 \\ \hline 84 \\ 206.5 \\ 139 \end{array}\right] \tag{8}$$

Note: Our Displacement model uses $\mathbf{P}_t^{Base}$ rather than $\mathbf{P}_t^{Disp}$. This renders our projected climate migrants demographically inert with no interaction with future component processes.

Our Amplification model differs in only a single way from our Displacement model. Rather than using $\mathbf{P}_t^{Base}$, this model uses $\mathbf{P}_t^{Amp}$, allowing all projected climate migrants to demographically interact with future component processes.

References

Bamber, J. L., Oppenheimer, M., Kopp, R. E., Aspinall, W. P. & Cooke, R. M. (2019), 'Ice sheet contributions to future sea-level rise from structured expert judgment', *Proceedings of the National Academy of Sciences* **116**(23), 11195–11200.

Black, R., Bennett, S. R. G., Thomas, S. M. & Beddington, J. R. (2011), 'Climate change: Migration as adaptation', *Nature* **478**, 447–449.

Buchner, B., Herve-Mignucci, M., Trabacchi, C., Wilkinson, J., Stadelmann, M., Boyd, R., Mazza, F., Falconer, A. & Micale, V. (2014), 'Global landscape of climate finance 2015', *Climate Policy Initiative* **32**, 1–38.

Chen, C. & Liu, L.-M. (1993), 'Joint estimation of model parameters and outlier effects in time series', *Journal of the American Statistical Association* **88**(421), 284–297.

Clark, W. A. & Maas, R. (2015), 'Interpreting migration through the prism of reasons for moves', *Population, Space and Place* **21**(1), 54–67.

Curtis, K. J. & Schneider, A. (2011), 'Understanding the demographic implications of climate change: Estimates of localized population predictions under future scenarios of sea-level rise', *Population and Environment* **33**(1), 28–54.

Davis, K. F., Battachan, A., D'Odorico, P. & Suweis, S. (2018), 'A universal model for predicting human migration under climate change: Examining future sea level rise in Bangladesh', *Environmental Research Letters* **13**.

De Lellis, P., Ruiz Marín, M. & Porfiri, M. (2021), 'Modeling Human Migration Under Environmental Change: A Case Study of the Effect of Sea Level Rise in Bangladesh', *Earth's Future* **9**(4).
URL: *https://onlinelibrary.wiley.com/doi/10.1029/2020EF001931*

Dedekorkut-Howes, A., Torabi, E. & Howes, M. (2020), 'When the tide gets high: A review of adaptive responses to sea level rise and coastal flooding', *Journal of Environmental Planning and Management* **63**(12), 2102–2143.

DeWaard, J., Hauer, M., Fussell, E., Curtis, K. J., Whitaker, S. D., McConnell, K., Price, K., Egan-Robertson, D., Soto, M. & Castro, C. A. (2021), 'User beware: Concerning findings from the post 2011–2012 us internal revenue service migration data', *Population Research and Policy Review* pp. 1–12.

Donner, S. D. & Webber, S. (2014), 'Obstacles to climate change adaptation decisions: A case study of sea-level rise and coastal protection measures in Kiribati', *Sustainability science* **9**(3), 331–345.

for Emergency Management and Homeland Security, C. (2018), 'The Spatial Hazard Events and Losses Database for the United States, Version 17.0 [Online Database]'.

Hauer, M. & Byars, J. (2019), 'Irs county-to-county migration data, 1990–2010', *Demographic Research* **40**, 1153–1166.

Hauer, M. E. (2017), 'Migration induced by sea-level rise could reshape the US population landscape', *Nature Climate Change* **7**(5), 321–325.

Hauer, M. E. (2019), 'Population projections for us counties by age, sex, and race controlled to shared socioeconomic pathway', *Scientific data* **6**(1), 1–15.

Hauer, M. E., Evans, J. M. & Mishra, D. R. (2016), 'Millions projected to be at risk from sea-level rise in the continental United States', *Nature Climate Change* **6**(7), 691–695.

Hauer, M. E., Fussell, E., Mueller, V., Burkett, M., Call, M., Abel, K., McLeman, R. & Wrathall, D. (2020), 'Sea-level rise and human migration', *Nature Reviews Earth & Environment* **1**(1), 28–39.

Hyndman, R., Athanasopoulos, G., Bergmeir, C., Caceres, G., Chhay, L., O'Hara-Wild, M., Petropoulos, F., Razbash, S., Wang, E. & Yasmeen, F. (2019), *forecast: Forecasting functions for time series and linear models*. R package version 8.10.
URL: *http://pkg.robjhyndman.com/forecast*

Hyndman, R. J. & Khandakar, Y. (2008), 'Automatic time series forecasting: the forecast package for R', *Journal of Statistical Software* **26**(3), 1–22.
URL: *http://www.jstatsoft.org/article/view/v027i03*

Hyndman, R., Koehler, A. B., Ord, J. K. & Snyder, R. D. (2008), *Forecasting with exponential smoothing: the state space approach*, Springer Science & Business Media.

IPCC & WMO, eds (1992), *Climate change: the 1990 and 1992 IPCC assessments, IPCC first assessment report overview and policymaker summaries and 1992 IPPC supplement*, IPCC, Geneve.

Kopp, R. E., Horton, R. M., Little, C. M., Mitrovica, J. X., Oppenheimer, M., Rasmussen, D. J., Strauss, B. H. & Tebaldi, C. (2014), 'Probabilistic 21st and 22nd century sea-level projections at a global network of tide-gauge sites', *Earth's future* **2**(8), 383–406.

Kopp, R. E., Horton, R. M., Little, C. M., Mitrovica, J. X., Oppenheimer, M., Rasmussen, D. J., Strauss, B. & Tebaldi, C. (n.d.), 'Probabilistic 21st and 22nd Century Sea-Level Projections at a Global Network of Tide-Gauge Sites', *Earth's Future* **2**, 383–406.

Kulp, S. A. & Strauss, B. H. (2019), 'New elevation data triple estimates of global vulnerability to sea-level rise and coastal flooding', *Nature communications* **10**(1), 1–12.

Lilleør, H. B. & Van den Broeck, K. (2011), 'Economic drivers of migration and climate change in ldcs', *Global environmental change* **21**, S70–S81.

López-de-Lacalle, J. (2019), *Tsoutliers: Detection of Outliers in Time Series*. R package version 0.6-8.

Marandi, A. & Main, K. L. (2021), 'Vulnerable city, recipient city, or climate destination? towards a typology of domestic climate migration impacts in us cities', *Journal of environmental studies and sciences* **11**(3), 465–480.

Matos-Moreno, A., Santos-Lozada, A. R., Mehta, N., Mendes de Leon, C. F., Lê-Scherban, F. & De Lima Friche, A. A. (2021), 'Migration is the Driving Force of Rapid Aging in Puerto Rico: A Research Brief', *Population Research and Policy Review* .
URL: *https://link.springer.com/10.1007/s11113-021-09683-2*

McGranahan, G., Balk, D. & Anderson, B. (2007), 'The rising tide: Assessing the risks of climate change and human settlements in low elevation coastal zones', *Environment and Urbanization* **19**(1), 17–37.

Mercer, J. H. (1978), 'West Antarctic ice sheet and CO 2 greenhouse effect: A threat of disaster', *Nature* **271**(5643), 321.
URL: *https://onlinelibrary.wiley.com/doi/10.1029/2020EF001931*

Molloy, R., Smith, C. L. & Wozniak, A. (2011), 'Internal migration in the united states', *Journal of Economic perspectives* **25**(3), 173–96.

Neumann, B., Vafeidis, A. T., Zimmermann, J. & Nicholls, R. J. (2015), 'Future Coastal Population Growth and Exposure to Sea-Level Rise and Coastal Flooding - A Global Assessment', *PLOS ONE* **10**(3), e0118571.

Nicholls, R. J. (2011), 'Planning for the impacts of sea level rise', *Oceanography* **24**(2), 144–157.

O'Neill, B. C., Tebaldi, C., Van Vuuren, D. P., Eyring, V., Friedlingstein, P., Hurtt, G., Knutti, R., Kriegler, E., Lamarque, J.-F., Lowe, J. et al. (2016), 'The scenario model intercomparison project (scenariomip) for cmip6', *Geoscientific Model Development* **9**(9), 3461–3482.

R Core Team (2019), *R: A Language and Environment for Statistical Computing*, R Foundation for Statistical Computing, Vienna, Austria.
URL: *https://www.R-project.org/*

Rahmstorf, S. (2007), 'A Semi-Empirical Approach to Projecting Future Sea-Level Rise', *Science* **315**(5810), 368–370.

Rigaud, K. K., de Sherbinin, A., Jones, B., Bergmann, J., Clement, V., Ober, K., Schewe, J., Adamo, S., McCusker, B., Heuser, S. et al. (2018), 'Groundswell'.

Robinson, C., Dilkina, B. & Moreno-Cruz, J. (2020), 'Modeling migration patterns in the usa under sea level rise', *PloS One* **15**(1), e0227436.

Rogers, A. (1966), 'The multiregional matrix growth operator and the stable interregional age structure', *Demography* **3**(2), 537–544.

Rogers, A. (1988), 'Age patterns of elderly migration: an international comparison', *Demography* **25**(3), 355–370.

Samir, K. & Lutz, W. (2017), 'The human core of the shared socioeconomic pathways: Population scenarios by age, sex and level of education for all countries to 2100', *Global Environmental Change* **42**, 181–192.

Seto, K. C. (2011), 'Exploring the dynamics of migration to mega-delta cities in Asia and Africa: Contemporary drivers and future scenarios', *Global Environmental Change* **21**, S94–S107.

Shen, S. & Gemenne, F. (2011), 'Contrasted views on environmental change and migration: The case of Tuvaluan migration to New Zealand', *International Migration* **49**, e224–e242.

Strauss, B. H., Kulp, S. & Levermann, A. (2015), 'Carbon choices determine US cities committed to futures below sea level', *Proceedings of the National Academy of Sciences* **112**(44), 13508–13513.

Swanson, D. A., Schlottmann, A. & Schmidt, B. (2010), 'Forecasting the population of census tracts by age and sex: An example of the hamilton–perry method in action', *Population Research and Policy Review* **29**(1), 47–63.

Sweet, W. V., Kopp, R. E., Weaver, C. P., Obeysekera, J., Horton, R. M., Thieler, E. R. & Zervas, C. (2017), 'Global and regional sea level rise scenarios for the United States'.

U.S. Fish and Wildlife Service (2012), 'National wetlands inventory website. u.s. department of the interior, fish and wildlife service, washington, d.c. http://www.fws.gov/wetlands/'.

US White House, ed. (2021), *Report on the Impact of Climate Change on Migration*, US White House, Washington DC.

Wilmoth, J., Zureick, S., Canudas-Romo, V., Inoue, M. & Sawyer, C. (2012), 'A flexible two-dimensional mortality model for use in indirect estimation', *Population studies* **66**(1), 1–28.

Xu, C., Kohler, T. A., Lenton, T. M., Svenning, J.-C. & Scheffer, M. (2020), 'Future of the human climate niche', *Proceedings of the National Academy of Sciences* **117**(21), 11350–11355.